**Eric C. Forrest[1]**
Primary Standards Laboratory,
Sandia National Laboratories,
Albuquerque, NM 87185
e-mail: ecforre@sandia.gov

**Sarah M. Don**
Department of Nuclear Science and Engineering,
Massachusetts Institute of Technology,
Cambridge, MA 02139
e-mail: sarahdon@alum.mit.edu

**Lin-Wen Hu**
Mem. ASME
Nuclear Reactor Laboratory,
Massachusetts Institute of Technology,
Cambridge, MA 02139
e-mail: lwhu@mit.edu

**Jacopo Buongiorno**
Mem. ASME
Department of Nuclear Science and Engineering,
Massachusetts Institute of Technology,
Cambridge, MA 02139
e-mail: jacopo@mit.edu

**Thomas J. McKrell**
Department of Nuclear Science and Engineering,
Massachusetts Institute of Technology,
Cambridge, MA 02139
e-mail: tmckrell@mit.edu

# Effect of Surface Oxidation on the Onset of Nucleate Boiling in a Materials Test Reactor Coolant Channel

*The onset of nucleate boiling (ONB) serves as the thermal-hydraulic operating limit for many research and test reactors. However, boiling incipience under forced convection has not been well-characterized in narrow channel geometries or for oxidized surface conditions. This study presents experimental data for the ONB in vertical upflow of deionized (DI) water in a simulated materials test reactor (MTR) coolant channel. The channel gap thickness and aspect ratio were 1.96 mm and 29:1, respectively. Boiling surface conditions were carefully controlled and characterized, with both heavily oxidized and native oxide surfaces tested. Measurements were performed for mass fluxes ranging from 750 to 3000 kg/m² s and for subcoolings ranging from 10 to 45°C. ONB was identified using a combination of high-speed visual observation, surface temperature measurements, and channel pressure drop measurements. Surface temperature measurements were found to be most reliable in identifying the ONB. For the nominal (native oxide) surface, results indicate that the correlation of Bergles and Rohsenow, when paired with the appropriate single-phase heat transfer correlation, adequately predicts the ONB heat flux. Incipience on the oxidized surface occurred at a higher heat flux and superheat than on the plain surface.* [DOI: 10.1115/1.4031503]

*Keywords: research reactor, thermal-hydraulics, boiling incipience, flow boiling, narrow channel*

## Introduction

The conversion of research and test reactors from high-enriched uranium (HEU) to low-enriched uranium (LEU) fuel is an ongoing international effort led by the U.S. National Nuclear Security Administration's Global Threat Reduction Initiative (GTRI). The conversion to LEU fuel poses numerous technical challenges for high-performance research reactors (HPRRs), including the MIT research reactor (MITR). Conversion to LEU fuel will result in a loss of reactor performance, as measured by the thermal neutron flux, due to hardening of the neutron spectrum. As such, power uprates are being evaluated in conversion studies. Maximum operating power is typically set by thermal-hydraulic limits. In the case of the MITR, the upper thermal-hydraulic operating limit is established by the limiting safety system setting (LSSS) criterion, which is ONB. This means that ONB must not be encountered anywhere on the cladding during either routine full-power operation with forced convection or low-power operation up to 100 kW with natural convection [1].

The MITR and other HPRRs are characterized by high-aspect ratio coolant channel geometries with gap thicknesses on the order of a few millimeters or less. However, correlations used in predicting ONB were developed for circular tube geometries without accounting for variation in surface conditions. In the case of the MITR, the correlation of Bergles and Rohsenow [2], in conjunction with the Dittus–Boelter correlation (McAdams version) [3], has been used to predict boiling incipience and therefore the maximum

allowable steady-state operating power. To date, the suitability of using these correlations in the MITR has not been experimentally verified. Better predictions of ONB in research and test reactor coolant channels could potentially enable power uprates following conversion to LEU fuel.

It is well known that the pool boiling properties, including the incipience point, depend on surface characteristics such as available cavity size and wettability [4–8]. However, few experimental studies have related surface effects such as oxidation to incipience under forced convection. Considering that fuel cladding may oxidize heavily during service, these effects should be explored further. In addition, some reactors such as the Advanced Test Reactor (ATR) prefilm their cladding to control pitting corrosion. Prefilmed cladding possesses different characteristics than surfaces with the native oxide.

This study investigates ONB in a prototypic MTR coolant channel, with dimensions based on the proposed LEU fuel assembly design for the MITR. The coolant channel is heated on one side only, representing a side channel in the MITR. In the MITR, the side channel is often limiting due to power peaking. Pressure and flow conditions tested are similar to those of the MITR under normal operating conditions. Several measurement techniques are used at each test condition to infer the impact on the observed incipience point. Data are collected for both the ONB heat flux and wall superheat on a plain surface (i.e., with native oxide) to assess the suitability of existing correlations such as that proposed by Bergles and Rohsenow. A heavily oxidized surface is also tested to determine the influence of wettability on ONB under forced convection.

---

[1]Corresponding author.
Manuscript received July 10, 2015; final manuscript received August 18, 2015; published online February 29, 2016. Assoc. Editor: Igor Pioro.

## Review of Theory and Prior Studies

The superheat required to sustain a vapor bubble may be derived from the Young–Laplace and Clausius–Clapeyron equations [9]. The Young–Laplace equation describes the pressure difference required to maintain mechanical equilibrium between two phases divided by an interface, such as that between a spherical vapor bubble and the surrounding liquid

$$P_{v} - P_{1} = \frac{2\sigma}{r} \tag{1}$$

where $r$ is the radius of curvature at the interface. The Clausius–Clapeyron equation may be written as

$$\frac{dP}{dT} = \frac{h_{fg}}{\Delta v T} \tag{2}$$

where $\Delta v$ is the specific volume difference between liquid and vapor. If the vapor can be treated as an ideal gas and $\Delta v \approx v_{v}$, then the above equation may be written as

$$\frac{dP}{dT} = \frac{h_{fg} P}{R T^{2}} \tag{3}$$

where $R$ is the specific gas constant. Taking $T_{1} = T_{sat}$, Eq. (3) can be integrated between $(P_{1}, T_{1})$ and $(P_{v}, T_{v})$

$$T_{v} - T_{sat} = \frac{R T_{v} T_{sat}}{h_{fg}} \ln\left(\frac{P_{v}}{P_{1}}\right) \tag{4}$$

and substituting in Eq. (1) gives the resultant superheat equation required to sustain a vapor bubble of radius $r_{ve}$ in equilibrium with the surrounding liquid

$$T_{v} - T_{sat} = \frac{R T_{v} T_{sat}}{h_{fg}} \ln\left(1 + \frac{2\sigma}{r_{ve} P_{1}}\right) \tag{5}$$

At low superheats or higher pressure (but still well below the critical point), the superheat equation may be simplified to

$$T_{v} - T_{sat} = \frac{2\sigma T_{sat}}{r_{ve} h_{fg} \rho_{v}} \tag{6}$$

Hsu and Graham [10] expand upon this criterion for stable bubble formation to identify the condition required for bubble growth out of a cavity in pool boiling. Their basic requirement is that the temperature at the tip of the bubble is at least equal to $T_{v}$ (Eq. (6)). Therefore, Hsu develops a transient model to account for the change in thickness of the thermal boundary layer near the wall during pool boiling: When the temperature at the tip of the bubble reaches $T_{v}$, the bubble is assumed to grow out of its nucleation site [11]. Investigations of incipience under forced convection are largely based on Hsu's original model, though in some respects forced convection models are simpler as they usually assume steady-state conditions.

For incipience under forced convection, models usually deal with a single, isolated bubble such that the thermal layer is within the laminar sublayer and can be treated as having a uniform and nonvarying thickness temporally. Heat transfer in the laminar sublayer is usually treated as occurring via conduction only, such that the temperature drop from the wall is linear

$$T_{1}(y) = T_{w} - \frac{q_{w}'' y}{k_{1}} \tag{7}$$

where $k_{1}$ is the thermal conductivity of the liquid in the laminar sublayer. The condition for incipience will vary depending on what assumption is taken for the bubble shape and the required thickness of the thermal layer. Figure 1 shows an illustration of different bubble models at incipience. As seen in the figure, the selection of bubble shape will affect the maximum height of the bubble above the heated surface. The superheated thermal layer meets
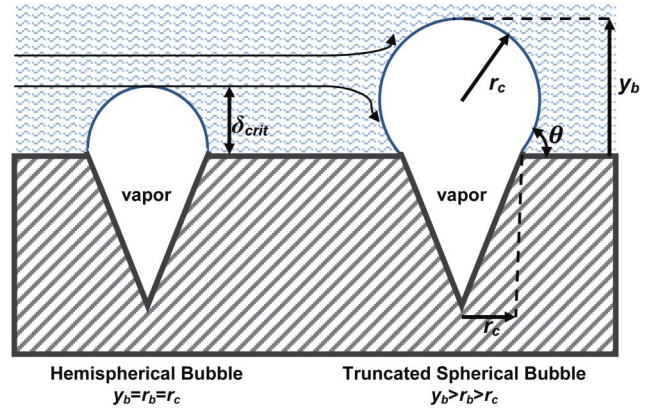


**Fig. 1 Hemispherical bubble model (left) and truncated sphere model (right)**

the minimum superheat requirement of Eq. (6) such that at the outer edge of the superheated thermal layer, the following equation is satisfied

$$T_{1}\big|_{y=\delta_{crit}} - T_{sat} = \frac{2\sigma T_{sat}}{r_{ve} h_{fg} \rho_{v}} \tag{8}$$

The required thickness, $\delta_{crit}$, for incipience depends on the criterion chosen with regard to the bubble height. In the original model of Hsu and Graham, this superheated thermal layer must be at least as thick as the bubble height, or $\delta_{crit} = y_{b}$. However, one can imagine that a streamline at a certain height would be deflected around the bubble, and the thermal layer thickness might therefore only need to reach this height. Several approaches have dealt with the issue of incipience under forced convection, with most of them building upon the model of Hsu and Graham.

**Bergles and Rohsenow.** In their 1964 work, Bergles and Rohsenow [2] treat the bubble shape as hemispherical, noting that, for a hydrophilic surface (contact angle < 90°), the bubble must pass through this state before growing outside the cavity. This state also matches the minimum radius of curvature, and the radius of the bubble can be considered equal to the cavity radius, such that

$$r_{b} = r_{c} \tag{9}$$

In their model, Bergles and Rohsenow assume that the bubble will grow when the superheat requirement is met at the top of the hemispherical bubble, or at $y = r_{b} = r_{c}$ from the nominal surface, though they note that this likely represents an upper limit. They acknowledge that if the liquid superheat criterion is met at a distance somewhat less than the bubble height ($r_{b}$ in this case), then there is net heat transfer to the bubble and it should still grow. Another important assumption taken by Bergles and Rohsenow is that a practical engineering surface will have a wide range of cavities, such that the optimum cavity size will be available for a given set of conditions. They approximate the analytical result by using a graphical solution method, arriving at the following expression:

$$q_{ONB}'' = 1083 P^{1.16} [1.8(T_{w} - T_{sat})]^{2.16/P^{0.023}} \tag{10}$$

where all variables are in SI units except for $P$, which is in bar. Equation (10) was determined for water over a pressure range of 1 bar < $P$ < 138 bar. Bergles and Rohsenow conduct experimental tests with degassed water in a small-diameter stainless steel tube (2.39 mm inner diameter) and an annulus to verify their analytical result, with good agreement found between the prediction and measured values.

**Satō and Matsumura.** Satō and Matsumura [12] approach the issue of incipience under forced convection analytically, initially assuming a complete sphere (not a truncated sphere) sitting on the surface. They select the height of the centerline of the spherical bubble as the required thickness for superheated layer meeting the condition of Eq. (8). In their analysis, they define the thickness of the entire superheated layer as

$$\delta_{shl} = \frac{k_1(T_w - T_{sat})}{q_w''} \tag{11}$$

The range of bubble sizes that can be supported at a given set of conditions will be

$$\frac{\delta_{shl}}{2} - \frac{1}{2}\sqrt{\delta_{shl}^2 - \frac{8k_1 T_{sat}(v_v - v_1)}{q_w'' h_{fg}}} \leq r_b$$
$$\leq \frac{\delta_{shl}}{2} + \frac{1}{2}\sqrt{\delta_{shl}^2 - \frac{8k_1 T_{sat}(v_v - v_1)}{q_w'' h_{fg}}} \tag{12}$$

The starting point of boiling is taken to be that requiring the minimum superheated layer, resulting in the following for the spherical bubble model:

$$q_{ONB}'' = \frac{k_1 h_{fg}}{8\sigma T_{sat}(v_v - v_1)}(T_w - T_{sat})^2 \tag{13}$$

Satō and Matsumura also consider the case of a hemispherical bubble, whereas here they use the height corresponding to the position of "the center of gravity of the critical bubble" for the superheated layer thickness, resulting in the following expression:

$$q_{ONB}'' = \frac{k_1 h_{fg}}{3\sigma T_{sat}(v_v - v_1)}(T_w - T_{sat})^2 \tag{14}$$

The former expression in Eq. (13) is typically referenced from the work of Satō and Matsumura. The latter assumption used for Eq. (14) predicts incipient boiling at about 40% lower superheat.

Satō and Matsumura also collect experimental data to support their analysis using a 10 mm × 7 mm stainless steel rectangular channel heated on two opposing sides. They perform tests with deaerated water for flow velocities ranging from 0.6 to 4.1 m/s and subcoolings from 3 to 70°C, finding reasonable agreement with results predicted from their analysis with a spherical bubble (Eq. (13)).

**Davis and Anderson.** Davis and Anderson [13] also approach the problem of incipience under forced convection analytically, assuming the following:

1. The bubble cavity, which develops at a surface cavity, has the shape of a truncated sphere.
2. Equilibrium theory can be used to predict the superheat required to satisfy a force balance on the bubble (Eq. (6)).
3. A bubble nucleus will grow if the temperature of the fluid at a distance from the wall equal to the bubble height is greater than the superheat required for bubble equilibrium in Eq. (8).
4. The bubble nucleus does not alter the temperature profile in the surrounding liquid.
5. Due to their small size, the bubble nuclei are found entirely within the laminar sublayer, and the temperature profile in the liquid can be determined from Eq. (7).

Davis and Anderson point out that the choice of streamline location is somewhat arbitrary, and that the selection at the top of the bubble, as both Hsu and Bergles and Rohsenow did, results in the limiting (maximum) superheat case for onset of boiling on a practical surface. They note that in their analysis, the bubble shape reduces to the hemispherical bubble when the contact angle is 90°, and also that the bubble may not grow much beyond the hemispherical bubble anyway, due to the strong shear forces which may act to sweep it from the wall [13]. Therefore, they consider the hemispherical bubble to have the greatest stability.

In the analysis, Davis and Anderson calculate the height of the bubble, bubble radius, and cavity radius to be related to the contact angle by

$$y_b = r_b[1 + \cos(\theta)] \tag{15}$$

$$r_c = r_b \sin(\theta) \tag{16}$$

Assuming the optimum surface cavity size is present, and also simplifying the problem by assuming a system at high pressure or fluid with low surface tension, Davis and Anderson arrive at the following relation between the heat flux and saturation superheat at ONB:

$$q_{ONB}'' = \frac{k_1 h_{fg} \rho_v}{8\sigma T_{sat}[1 + \cos(\theta)]}(T_w - T_{sat})^2 \tag{17}$$

Note that when a contact angle of 90° is assumed, Eq. (17) essentially reduces to Satō's prediction assuming a perfectly spherical bubble sitting on the surface (Eq. (13)). A bubble contact angle of 90° implies a hemispherical bubble, but the same end result is obtained due to the choice of different streamline locations.

Davis and Anderson compare their prediction to the data of prior studies and reach several interesting conclusions. They note that inconsistencies between theoretical analyses and empirical data are primarily due to characteristics of the heat transfer surface. Specifically, they note that some studies used very smooth surfaces, which likely lacked cavities of the optimum size or active cavities altogether, thereby leading to higher superheats for initial nucleation. In addition, they note that the method for identifying incipience will affect the result, stating that inaccuracies will likely result from visual identification techniques. They also point out that since the optimum cavity sizes under normal circumstances can be on the order of 1 $\mu$m, which is below the magnitude that can be studied with optical instruments, considerable difficulty may be associated with studying active cavities and bubble nuclei on heat transfer surfaces.

**Kandlikar et al.** A more recent study by Kandlikar et al. [14,15] reviews several models for boiling incipience under forced convection and proposes one where the necessary thickness of the superheated liquid layer must be greater than or equal to the height of the stagnation point. Kandlikar states that the relevant contact angle in Fig. 1 is the receding contact angle. In his review, he reminds us that Hsu used a streamline at the top of a truncated spherical bubble, and that Hsu assumed that $y_b = 1.6 r_b$, which essentially equates to a receding contact angle about 50°. Kandlikar, however, assumes that a streamline can be taken at a lower point on the bubble, arguing that any streamlines above a stagnation point will be deflected above and around the bubble. For receding contact angles, $\beta$, from 20° to 60°, Kandlikar states that the height of the stagnation point, $y_{stag}$, will be

$$y_{stag} = 1.1 r_b = 1.1 \frac{r_c}{\sin(\beta)} \tag{18}$$

where $\beta$ is the dynamic receding contact angle. According to Kandlikar's model, the range of active cavity sizes on a surface that can support nucleation for a given set of conditions will be

$$\{r_{c,min}, r_{c,max}\} = \frac{\delta_{th,eq}\sin(\beta)}{2[1 + \cos(\beta)]}\left(\frac{T_w - T_{sat}}{T_w - T_b}\right)$$
$$\times \left[1 \mp \frac{1}{2}\sqrt{1 - \frac{8.8 T_{sat}(T_w - T_b)}{\rho_v h_{fg}\delta_{th,eq}(T_w - T_{sat})^2}}\right] \tag{19}$$

It is important to note that the thermal layer thickness, $\delta_{th,eq}$, used by Kandlikar is not the thickness of the superheated layer, as in

Eq. (11), but rather, an equivalent thickness of the entire thermal layer assuming a linear temperature profile such that

$$\delta_{\text{th,eq}} = \frac{k_1}{h} = \frac{k_l(T_w - T_b)}{q_w''} \qquad (20)$$

where $h$ is the heat transfer coefficient for forced convection prior to incipience. While this assumption of a linear temperature profile for the entire thermal layer is not accurate for transition and turbulent flows, it can be seen in Eq. (19) that this thermal layer thickness can be reduced to the superheated layer thickness by combining with the wall superheat terms. The final relation between wall superheat and surface heat flux at the point of incipience for Kandlikar's model is

$$q_{\text{ONB}}'' = \frac{k_1 \sin(\beta)}{1.1 r_c} \left[ (T_w - T_{\text{sat}}) - \frac{2\sigma T_{\text{sat}} \sin(\beta)}{\rho_v h_{\text{fg}} r_c} \right] \qquad (21)$$

Experimental studies were carried out by Kandlikar et al. [15] in a 3 mm × 40 mm rectangular channel with a 10 mm diameter circular heater flush with the lower wall. Tests were conducted at essentially atmospheric pressure with distilled water that was thoroughly degassed. It should be noted that given the small size of the heater, flow was not likely fully developed thermally in their tests. They measure ONB with wall temperature and also attempt to identify incipience visually using a high-speed video camera/microscope setup. However, tests are conducted at relatively low flows, with a maximum Reynolds number of 5068 and mass flux of 355 kg/m² s. Therefore, the flow velocities of their study are about 1/10th that relevant to conditions in the MITR during steady-state operation.

Nonetheless, the experimental study yields useful information regarding visual identification of incipience. At a subcooling of about 40°C and Reynolds number of 1267, bubbles reach a maximum diameter of 78 μm before departure, whereas for a Reynolds number of 2280, the maximum departure diameter was only 56 μm. At a subcooling of about 20°C and Reynolds number of 1664, observed bubble departure diameters ranged from 80 to 90 μm. They also observe bubble growth rates, noting that the influence of subcooling and flow rate is quite complex. A decrease in the subcooling leads to higher growth rates, which they note makes it quite difficult to capture bubble growth when the subcooling is less than 20°C. For a subcooling of 20°C and Re = 1664, Kandlikar et al. observe bubble growth times of 22 ms. At higher flow rates, the bubble growth period is even more rapid, and they note frame rates in excess of 1,00,000 Hz might be required to capture the rapid bubble growth and departure of very small bubbles. They conclude that under certain conditions, bubble growth is so strongly dependent on subcooling and mass flux that bubble activity could not be captured, despite heat transfer data indicating the presence of nucleation. They hypothesize the possibility of small bubbles (5–10 μm in diameter) being ejected from cavities at high speeds, in excess of 6000 bubbles per second at a given nucleation site, and therefore going undetected by visual measurement techniques.

**Other Studies.** A number of other relevant studies have been conducted for ONB under forced convection. In a 1986 study supporting a power uprate of the JRR-3 following conversion to LEU fuel, Sudo et al. [16] investigate the ONB in a narrow channel geometry. Their 2.25 mm × 50 mm rectangular channel simulated the coolant channel of a MTR. Data were collected for upflow with pure water at 1.2 bar and inlet temperature of 34.9°C. The maximum flow velocity was 1.48 m/s for onset of boiling measurements, with a maximum corresponding heat flux of 800 kW/m². Sudo et al. state the Bergles–Rohsenow correlation gives a good estimate of ONB, corresponding to the lower limits of measured ONB. They also observed no difference in boiling onset for upflow or downflow at the conditions tested. Lastly, they claim that there is no significant hysteresis in the boiling curve with operational history, i.e., whether the heat flux is increasing or decreasing. The study by Sudo et al. has been the motivation for continued usage

of the Bergles–Rohsenow correlation for the MITR and is cited in the current Safety Analysis Report [1].

Several recent studies investigate the ONB in narrow annuli [17] and narrow rectangular channels [18,19] at low flow velocities, with mass fluxes in these studies being below 840, 603, and 145 kg/m² s, respectively.

## Experimental

**Measurement Considerations for Identifying ONB.** The ONB is the point on a heated surface when a vapor embryo is able to grow above the surface (outside of a cavity) and be sustained in equilibrium with the surrounding liquid. The method used to experimentally identify this point will have a significant effect on the reported heat flux and superheat. Several techniques exist, and depending on the conditions, may yield drastically different results for ONB. Even using the same technique between experiments may yield significantly different results depending on the exact criteria used. In general, methods for identifying ONB will rely on at least one of the measurement techniques discussed below.

*Surface Temperature.* Techniques relying on temperature measurement attempt to determine the point of boiling incipience by analyzing the change in the surface heat transfer coefficient. As bubbles grow on the surface, they may collapse (due to condensation heat transfer) and result in a new bubble being formed at the same location. The heat transfer coefficient will increase due to the latent heat required to form the vapor bubble, the increased convective motion at the surface, and the quenching effect required to heat the subcooled liquid that replaces the vapor bubble. Surface temperature measurement using thermocouples typically only provides local information at or about where the thermocouple is placed, with infrared thermography being the only means to achieve full-field temperature measurements. Therefore, the point at which a detectable change in the heat transfer coefficient occurs will likely be slightly beyond ONB. This is because many sites must become active, and the bubble must grow large enough to either collapse or depart to result in a measurable effect on the heat transfer coefficient. The criteria used to determine the ONB point are not always clearly stated, leading to inconsistencies between studies. For example, identifying incipience as the point at which the heat transfer coefficient changes by 5% will yield a different result than requiring a 10% change in the heat transfer coefficient. Simply identifying the point on the boiling curve where a significant change in slope occurs may not be adequate, as the "knee" of the boiling curve may extend over a wide range of superheat, especially at higher mass fluxes. Lastly, the uncertainty in the surface temperature and heat flux measurement must be carefully accounted for, to ensure that the change in the heat transfer coefficient at the expected point of onset is statistically significant.

As the current MITR safety analysis relies upon the correlation proposed by Bergles and Rohsenow, it is important to understand how ONB was identified in their experiments used to support their analytical correlation. They used temperature measurements to identify incipience, and while visual identification was originally intended to support this, it was found that incipient boiling occurred below the visual threshold. It is also critical to understand the exact temperature criterion used to identify incipience; otherwise, a direct comparison to their results is not possible. While the journal publication [2] does not go into great detail, their report for the Air Force [20] describes the approach in-depth. Forced convection data were collected, and the resultant boiling curves were partitioned into the forced convection single-phase and boiling heat flux components. The single-phase component of the heat flux was determined from a fit to their single-phase data. While Bergles and Rohsenow [20] do not explicitly specify a set breakpoint for choosing ONB, it would appear from the figure that when the boiling component of the heat flux exceeds ~7.5%, boiling incipience is declared to occur. Bergles and Rohsenow themselves note that exact

determination of ONB under forced convection is a matter of judgment, with incipience occurring over a spread of at least 2.5°C in the wall superheat.

*Coolant Channel Pressure Drop.* Phase change in a heated channel will influence the pressure drop of the system by altering the friction factor and increasing the acceleration pressure drop. Therefore, pressure drop measurements are one possible way of determining ONB. In tests to measure the onset of flow instability, Kennedy et al. [21] state that on the characteristic pressure drop versus flow rate curve, the point at which the gradients for the heated and unheated curves become noticeably different should correspond to ONB. However, gradual changes in liquid properties with heating, along with dimensional changes that may be non-negligible for very narrow channels, will also result in changes in the pressure drop as the heat flux is increased in the channel. The relative effect of boiling on pressure drop will also depend on the subcooling and flow conditions. For high subcooling where the bubbles collapse immediately and do not depart, the relative effect on pressure drop is more subtle. Similarly, at high mass fluxes where inertia forces dominate, the relative effect of boiling on pressure drop will be, at first, less noticeable. Therefore, at the onset of boiling, there will not be a sharp rise in the pressure drop, but more of a gradual transition, meaning there is also some subjectivity in applying this technique.

In conducting experiments, it was noted in many cases that the rise in pressure drop with increasing heat flux was so gradual as to preclude objectively identifying onset of boiling using this method. However, a sharp increase in the relative standard deviation of the pressure drop signal with time was noted at the onset of boiling. This method of identifying incipience appeared to work equally well regardless of subcooling, providing a global measurement for first onset of boiling in the channel, even if it occurred at a location without temperature measurement, such as at the very exit of the channel. The increased oscillation in the pressure signal with time is likely due to the rapid growth and collapse of bubbles at the surface.

*Visual.* Visual identification techniques, in which a sight glass or viewing window on the heated flow section allows for optical observation to determine when bubbles form on the surface, have been used, or attempted, in a number of studies [2,15,17–19,21], including the current one. In principle, the technique should be quite simple, with the appearance of a bubble growing outside of a cavity indicating the incipience point. However, in practice, visual identification methods are neither reliable nor consistent. Under relevant conditions in water, the optimum cavity size for nucleation is on the order of several $\mu$m. Therefore, on a practical engineering surface which possesses cavities in this range, these will be the first cavities to nucleate. Assuming a hemispherical bubble, as did Bergles and Rohsenow, the bubble diameter will be the same as the cavity diameter, or several $\mu$m wide. Therefore, the optical system must have a spatial resolution that is even smaller than 2–3 $\mu$m. The theoretical spatial limit for optical techniques, defined by the diffraction limit (which is set by the wavelength of light), is about 0.25 $\mu$m. In practice, the best optical systems for high-speed visualization might be able to achieve spatial resolutions of a few $\mu$m, which is still not adequate for the expected bubble diameter and height at the exact moment of incipience.

According to Collier and Thome, when bubbles are visible, a much higher heat flux (two-and-one-half times) is required to permit visual detection versus improvement in the heat transfer coefficient [22]. Under these circumstances at incipience, bubbles at the wall are likely too small to observe optically. This could explain the recent studies using visual means reporting ONB occurring at much higher temperatures and heat fluxes than predicted by Bergles and Rohsenow. One of the test sections used in the original study by Bergles and Rohsenow was a Pyrex annulus, presumably to permit visual identification of incipience, though no visual characterization is mentioned [2]. A detailed report [20] explains that visual identification of incipience was not possible.

In this study, it was confirmed that initial incipience was practically impossible to view at mass fluxes greater than 750 kg/m² s and subcooling greater than 25°C. When voiding was visible, it was at much greater heat fluxes and shortly before the onset of flow instability. At the lowest mass flux of this study (750 kg/m² s) and a subcooling of 25°C, dispersed bubble sizes following onset of boiling were on the order of 80 $\mu$m in diameter. Increases in mass flux and subcooling will make the bubble size near the incipient heat flux substantially smaller, and well below the optical resolution for visualization.

Ultimately, the identification of ONB using temperature measurement is expected to be most reliable. When comparing results to existing correlations, the least amount of error will result if the same identification technique is utilized. In most cases, prior correlations were supported using temperature measurement techniques. Visual techniques are only possible with very high resolution equipment at certain flow conditions and are still subject to the experimentalist's bias. Measurement of the pressure fluctuation has the potential to provide a more quantitative assessment and yield a "global" measurement, but the main drawback is that it does not provide an associated wall temperature.

Inconsistent results in the literature may be attributed to different techniques and/or criteria used to identify the ONB. Most studies do not provide details regarding surface conditions such as roughness. In addition, operating procedures for experiments to measure the incipience point may differ between studies. Dissolved gas content is known to affect boiling incipience [23–25] and is difficult to control. Substantial amounts of dissolved gas in the fluid and cavities on the heating surface can lead to "pseudo-boiling," where a surface may off-gas noncondensable gas bubbles as its temperature increases, even if the surface is below the saturation temperature. This bubbling of noncondensable gases from the surface could potentially be mistaken for actual boiling. In the study of Bergles and Rohsenow, their system water was degassed to less than 1.5 cm³ of air per liter for all runs, to eliminate premature bubbling. Operational history and whether the onset of boiling point is measured while ramping the heat flux up or decreasing it may also affect the measured heat flux and superheat at which incipience occurs.

**Apparatus.** The experimental apparatus consisted of a simulated MTR coolant channel heated on one side with a viewing window on the front face. The flow loop accommodating the test section provided conditions matching those found in the MITR during normal operation. A LaVision Phantom v12.1 high-speed camera was used to capture incipience and subsequent boiling, when possible, at rates up to 20,000 fps. The optical setup yielded a pixel resolution of about 20 $\mu$m. Details of the test section, compared to MITR parameters, are listed in Table 1. Note that since

Table 1 Parameters for the test section employed in this study compared to the proposed coolant channel for the MITR LEU core

| Parameter | Test section | MITR coolant channel |
| --- | --- | --- |
| Channel gap | 1.96 mm | 1.96 mm |
| Channel width | 55.9 mm | 55.9 mm |
| Channel length | 483 mm | 584 mm |
| Hydraulic diameter | 3.91 mm | 3.91 mm |
| Heated width | 51.0 mm | 52.9 mm |
| Heated length | 305 mm | 559 mm |
| Inclination | 90° (vertical upflow) | 90° (vertical upflow) |
| Outlet pressure | up to 3.1 bar | 1.3 bar |
| Inlet temperature | up to 99°C | 42°C |
| Mass flux | up to 7000 kg/m² s | 2750 kg/m² s |
| Surface heat flux | up to 3.8 MW/m² | 231 kW/m² (Normal operation) |
| Confinement number | 0.65–0.71 | 0.68–0.69 |
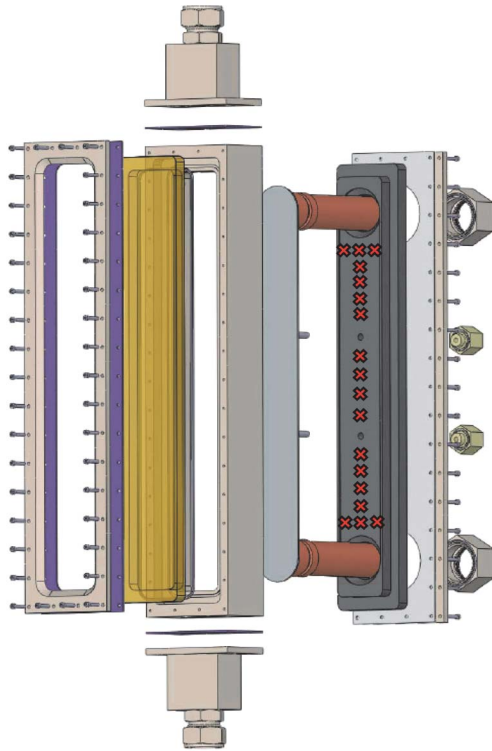
**Fig. 2 Exploded view of the test section, with thermocouple locations indicated by X's**

the confinement number, Co, is greater than 0.5, boiling is considered confined by the channel geometry. Figure 2 shows an exploded view of the test section with temperature measurement locations. A complete description of the experimental flow loop, test section, and measurement equipment is provided in Ref. [26].

An uncertainty analysis was performed for the experimental system to estimate total uncertainties for all measured and calculated parameters. Fundamental measurement uncertainties of the system are summarized in Table 2 and were propagated using the method described by Kline and McClintock [27]. Dimensional tolerances were accounted for in the uncertainty analysis. Error associated with the heat flux step and partition method was included in the final ONB heat flux uncertainty.

**Surface Preparation.** The surface finish of the channel was carefully controlled, with the heater plate prepared to match the roughness expected on actual MTR cladding. While it was not possible to exactly replicate the texture of MTR cladding due to the

different fabrication process, the objective was to obtain an arithmetic surface roughness, $R_a$, equivalent to that measured for MTR cladding surfaces. The surface finishing techniques were shown to be very repeatable by roughness measurements at various locations on different coupons prepared in a nominally identical fashion. The technique ultimately selected involved wet-sanding of the as-received surface with 120-grit SiC sandpaper using a figure-eight pattern, resulting in a uniform surface free of gouges or deep scratches. Before installation into the flow facility, the heater surface was sonicated in acetone for 15 min to remove any remaining grit, rinsed with ethanol, wiped with nonscratching lint-free tissue, followed by a final rinse with DI water and blown dry with clean, compressed nitrogen.

The plate used for the oxidized surface studies was fabricated and finished in the same manner as that for the nominal surface studies. The plate was then placed in a ThermoScientific Thermo-Lyne box furnace, which was preheated to 600°C. The plate was heated in air at atmospheric pressure for 4 hr, at which point it was removed from the furnace. The surface of the plate exhibited a blue/brown tint after removal, as a result of the thin-film interference of the thin oxide film formed on the surface. Prior to final installation in the test section, the plate was cleaned with acetone, ethanol, and water. Between every boiling test, the surface of the plate was wiped down with ultrapure ethanol and rinsed with DI water to remove any loose deposits or corrosion products. The nominal plate and oxidized plate are shown in Fig. 3.

**Test Procedure.** All tests were conducted with DI water, where the measured resistivity was greater than 15 MΩ cm. Water was degassed by reducing the system pressure and heating to 80°C for several hours. The surface of the plate was degassed prior to every test by boiling vigorously for at least 30 min at reduced pressure, with noncondensable gases being frequently vented from the system. The system pressure was increased and the fluid temperature decreased following degassing to collapse any entrapped vapor on the heater surface. The dissolved oxygen content of the water was measured using a Eutech Alpha DO 500 probe at the end of each test by diverting the full flow through the dissolved oxygen measurement loop and was typically around 4.0 ppm or less.

ONB tests were conducted by maintaining a fixed mass flux through the test section, while increasing the heat flux in a stepwise manner. Tests were conducted by keeping the test section outlet pressure at a fixed value of 1.3 bar and maintaining the test section inlet temperature at a fixed value, similar to the actual conditions in the MITR. Therefore, as the heat flux was increased, the bulk fluid temperature rise along the test section would increase, thereby resulting in a higher bulk outlet temperature with each step. The heat flux was held at each step long enough to reach equilibrium conditions (typically around 30 min), determined when the plate temperatures reached steady-state values. Local backside temperatures were measured using Type E thermocouples that were thermally

**Table 2 Summary of fundamental measurement uncertainties for the thermal-hydraulic facility and test section**

| Parameter | Total uncertainty | Notes |
|---|---|---|
| Primary current, $I_P$ | $\pm 1\% \, \text{FS} = \pm 60 \, \text{A}$ | For current transducer. Offset corrected separately |
| Voltage drop, $V_E$ | $\pm (0.005\% \text{ of reading} + 4 \times 10^{-6}) \, \text{V}$ | Data acquisition system voltage channel |
| Current signal, $I$ | $\pm 5.5 \times 10^{-5} \, \text{A}$ | Data acquisition system 4–20 mA channel. |
| Type E TC temperature, $T$ | $\pm 0.297°C$ | Total uncertainty of least accurate thermocouple on backside of heater plate |
| RTD temperature, $T_{in}$, $T_{out}$ | $\pm 0.156°C$ | Total uncertainty of least accurate RTD used for inlet and outlet fluid temperature measurements |
| Differential RTD temperature, $\Delta T$ | $\pm 0.052°C$ | Maximum deviation + random uncertainty of inlet and outlet RTD. |
| Primary flow rate, $Q_p$ | $\varepsilon_m = \pm 5.68 \, \text{gpm/A}$ $\varepsilon_b = \pm 0.068 \, \text{gpm}$ | Uncertainty in slope and intercept of fitted calibration curve |
| Absolute pressure, $P$ | $\pm 0.25\% \, \text{FS} = \pm 0.125 \, \text{psia} \, (\pm 0.0086 \, \text{bar})$ | Includes linearity, repeatability, and hysteresis |
| Differential pressure, $P$ | $\pm 0.25\% \, \text{FS} = \pm 0.025 \, \text{psia} \, (\pm 0.0017 \, \text{bar})$ | Includes linearity, repeatability, and hysteresis |

Uncertainties represent 95% confidence bounds.

Fig. 3 Photograph of nominal plate (top) and plate follow-ing 600°C oxidation in air (bottom)

bonded but electrically insulated so as not to affect the local heat flux. Temperatures were measured at 5 s intervals, whereas the pressure drop was measured at 50 ms intervals.

Data were first collected at lower heat fluxes such that the single-phase component of the heat flux could be determined for each test at each location by fitting a line to the data, where the wall temperatures were below the saturation temperature. The total heat flux at each thermocouple location was partitioned into single-phase forced convection and boiling components. The inception of first significant boiling was identified in the empirical studies as the first point, which met all of the following criteria:

1. The calculated surface temperature is greater than the local saturation temperature.
2. The partitioned boiling heat flux is greater than 7.5% (approximate value assumed by Bergles and Rohsenow from inspection of their graphs).
3. The measurement uncertainty in the heat flux at that point is less than the partitioned boiling heat flux.

The results for forced convection boiling tests for mass fluxes ranging from 750 to 3000 kg/m$^2$ s and subcoolings from 15 to 40°C are reported.

## Results for ONB

**Boiling Curves (From Temperature Measurements).** Partial forced convection boiling curves were calculated from measured data at each thermocouple location using local conditions. Several curves are shown in Fig. 4 at the lowest mass flux condition of 750 kg/m$^2$ s, with error bars for TC13 indicating 95% bounds of the measurement uncertainty and representing values typical for the other thermocouple locations. Figure 5 shows a partial forced convection boiling curve for $G = 3000$ kg/m$^2$ s with an inlet bulk temperature of 80°C. Considering that pressure and bulk fluid temperature varied along the length of the channel, boiling would typically initiate toward the outlet with the fluid remaining in the single-phase regime further upstream. Therefore, thermocouple locations toward the outlet of the channel that experienced fully developed flow (i.e., that were not in the "exit region") were used to determine the ONB point.
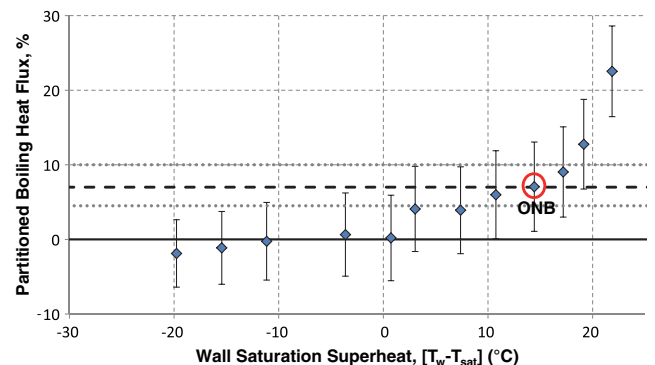
The ONB point was determined using the method of Bergles and Rohsenow, as outlined earlier, and is demonstrated in Fig. 6.
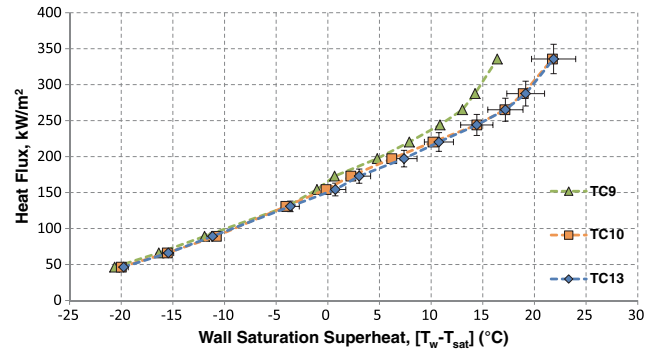


Fig. 4 Partial boiling curves based on local temperature measurements for $G = 750$ kg/m$^2$ s, $T_{bulk,in} = 80°C$, and $P_{out} = 1.3$ bar
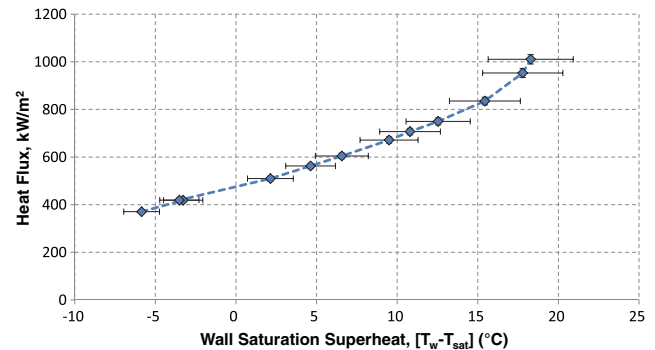


Fig. 5 Partial forced convection boiling curve for $G = 3000$ kg/m$^2$ s, $T_{bulk,in} = 80°C$, and $P_{out} = 1.3$ bar



Fig. 6 Partitioned boiling heat flux for TC13 from the forced convection boiling curve in Fig. 4. A boiling heat flux partition of 7.5% was used to determine the ONB

The same metric was consistently applied for all tests. As shown in Fig. 6, a slight change in the partition heat flux may lead to a substantially different assessment of ONB, indicating that the uncertainty in ONB identification is much larger than the measurement uncertainty in the heat flux. Therefore, the 95% uncertainty in the ONB heat flux was estimated by using neighboring data points, where the heat flux partition differed by at least ±2.5%. This uncertainty accounts for both the error induced by a finite heat flux step size and also attempts to account for the underlying uncertainty in the partition method. Considering the measurement criteria and that a change of ±2.5% in the partition may not lead to the same
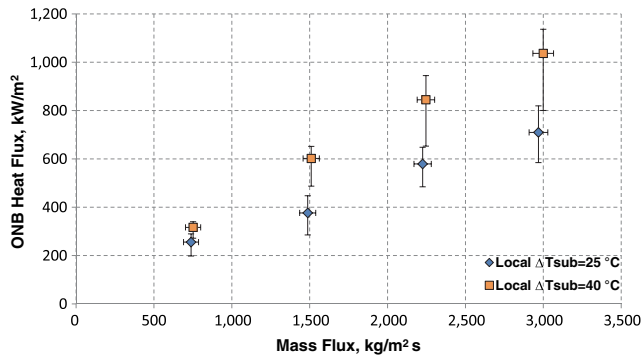
**Fig. 7 Measured heat flux at the ONB, determined using local temperature measurement and the partition heat flux method**



**Fig. 9 Channel pressure drop and relative standard deviation of pressure drop-time signal for $G = 750$ kg/m$^2$ s and $T_{bulk,in} = 90°C$**

increase or decrease in the ONB heat flux, the estimated uncertainty in the ONB heat flux was not necessarily symmetric about the determined value.

Average results for all conditions on the nominal surface where the temperature measurement criteria were applied (i.e., the partition heat flux method) are summarized in Fig. 7. Note that repeatability tests were carried out to demonstrate the measured heat flux at ONB was consistent. The local surface temperature at the incipient point was also recorded in order to calculate the saturation superheat required for nucleation. Similar tests were conducted for the heavily oxidized surface at one inlet subcooling. Results using the partition heat flux method for the heavily oxidized surface are summarized in Fig. 8.

**Pressure Fluctuation.** Pressure measurements could also be used to determine the heat flux at which the ONB occurred. The change in the pressure drop at ONB was typically quite small, which is expected, especially under subcooled conditions. Therefore, the time-averaged pressure drop at each heat flux was not a suitable criterion for determining the ONB heat flux in the channel. However, as the heat flux increased, the fluctuation in the pressure signal with time became significant and can therefore be used as the means for identifying first ONB in the channel. An example of the measured pressure drop at each heat flux step, along with the associated fluctuation in the pressure drop signal, is provided in Fig. 9. The relative standard deviation of the pressure signal with time was used as a measure of the pressure signal fluctuation. The advantage of this approach is that it offers a means of determining first onset of boiling in the channel and is not tied to a specific thermocouple
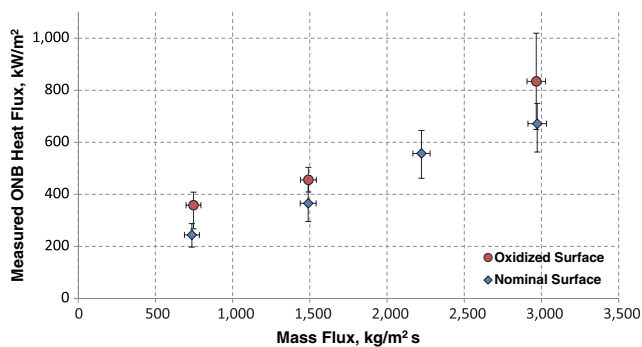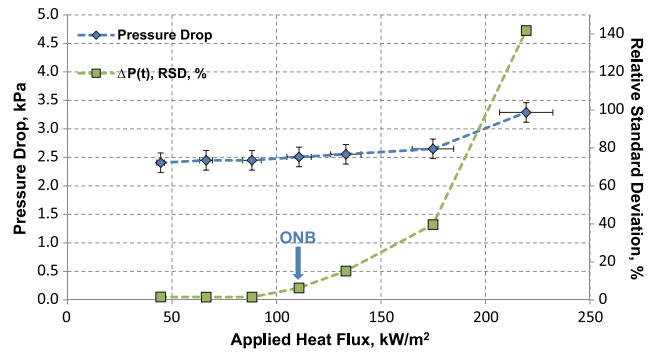
position. Therefore, if incipience was to occur first at the channel exit, which is generally expected, or at any other location where the thermocouples could not be placed (such as away from the axial centerline), the pressure fluctuation method would be able to capture the occurrence. The serious drawback of this method is that the local wall temperature at the onset of boiling cannot be measured. It is the superheat itself, and not the heat flux, which leads to incipience on the surface. However, the measured saturation superheat at the onset of boiling is highly sensitive to the ONB selection criteria and subject to large uncertainty. The value of correlating the ONB heat flux using the experimental wall temperature is somewhat diminished. Instead, the surface temperature can be predicted using the appropriate single-phase correlation, and the comparison of data can be made in this manner. Figure 10 summarizes all measured heat fluxes at ONB using the pressure fluctuation method. Note that at the lowest subcooling, where the bulk inlet temperature was about 90°C, onset of boiling always started at the channel exit, where thermocouples could not be installed due to the electrode clamp. The low subcooling condition was associated with flow instabilities shortly following ONB at the channel exit.

**Visual.** It was generally not possible to visualize vapor bubbles at or shortly after incipience under most flow conditions for reasons discussed previously. For these tests, flow appeared to transition from single-phase to slug/churn flow almost immediately, though pressure and temperature measurements clearly indicated that boiling was occurring prior to reaching this point. However, in the test cases at the lowest mass fluxes, bubbles were visible near incipience, where they departed with some fraction surviving for a short time in the flow before collapsing.

In the few test cases where vapor bubbles were visible at or near the incipience point, the bubbles were rather small and nearly



**Fig. 8 Comparison of the measured ONB heat flux for the oxidized and nominal surfaces as a function of mass flux. Tests shown are for an inlet temperature of 80°C, and an outlet pressure of 1.3 bar**
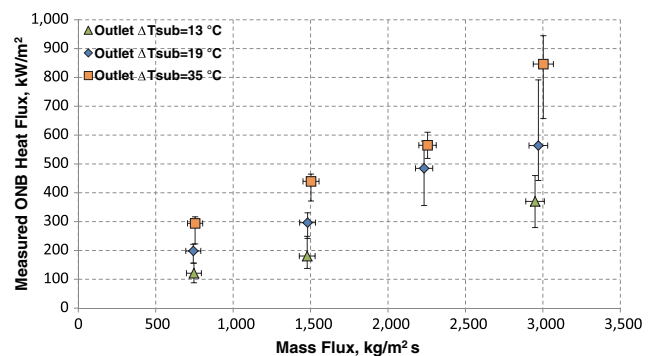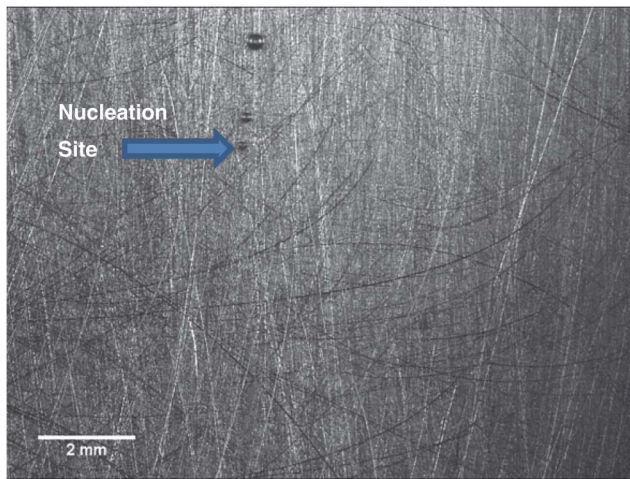


**Fig. 10 ONB heat flux at channel outlet as determined from pressure measurement fluctuations**

**Fig. 11  Active nucleation site shortly after incipience point. $G = 750$ kg/m$^2$ s and $T_{bulk,in} = 90°C$**

impossible to visualize without video playback (i.e., they were not distinguishable in still frames). In only one case at the lowest subcooling (10.7°C) and mass flux (740 kg/m$^2$ s) tested could an actual nucleation site be visualized shortly after the point of incipience. This is shown in Fig. 11. At heat fluxes beyond initial incipience, bubbles in the free stream were greater in number and larger in size, as seen in Fig. 12, though this occurrence shortly preceded the onset of flow instability. The flow regime can best be described as bubbly about the center of the channel, with vapor plugs becoming more prominent at the channel edges as heat flux was increased, likely indicating direct evaporation was taking place at the edges. Toward the outlet of the channel as heat flux was increased further, vapor engulfed a significant fraction of the channel, with the flow regime best being described as slug/churn flow.

Incipience points identified visually with the aid of high-speed video are summarized in Table 3. Note that for most cases, the visual technique could not be used due to the prohibitively small bubble size at incipience. In these cases, the working fluid and surface were degassed prior to tests. Using water with high-dissolved gas content may lead to the erroneous visual identification of nucleation due to off-gassing of noncondensables during surface heating. Bubbles that are seen leaving the surface may consist entirely of noncondensable gases or a mix of gas and vapor and
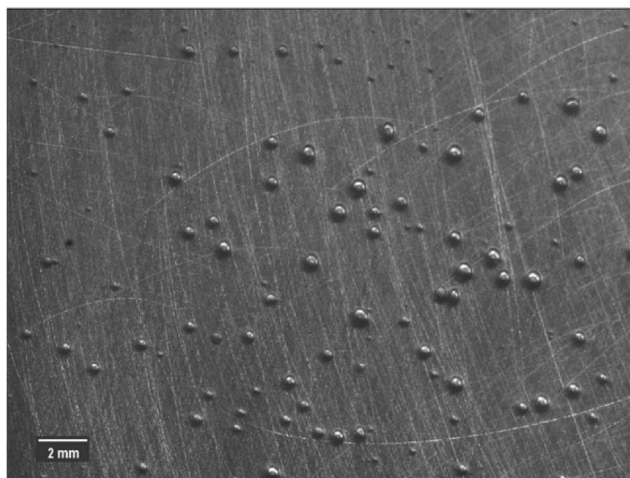


**Fig. 12  Bubbly flow in channel. $G = 750$ kg/m$^2$ s and $T_{bulk,in} = 90°C$**

**Table 3  Summary of visual observations for ONB using high-speed video recordings**

| Mass flux (kg/m$^2$ s) | Subcooling (°C) | ONB heat flux, heat flux partition (kW/m$^2$) | ONB heat flux, visual observation (kW/m$^2$) |
|---|---|---|---|
| 740 | 10.7 | Not measured | 220 |
| 740 | 21.2 | 267 (199, 292) | 246 |
| 750 | 39.6 | 317 (272, 340) | 272 |
| 1460 | 10.7 | Not measured | Not visible |
| 1480 | 22.8 | 442 (387, 497) | Not visible |
| 1510 | 40.7 | 602 (487, 652) | Not visible |
| 2220 | 24.6 | 557 (462, 645) | Not visible |
| 2230 | 23.4 | 651 (508, 794) | Not visible |
| 2970 | 26.1 | 748 (607, 889) | Not visible |
| 3000 | 43.0 | 1036 (801, 1136) | Not visible |

Under most conditions, vapor bubbles could not be seen at or near the point of incipience. Values in parentheses indicate the experimentalist's 95% confidence interval estimate.

therefore are not indicative of actual boiling, but rather, "pseudo-boiling," as pointed out by McAdams [23] and later Bergles and Rohsenow [20]. This was observed during surface degassing prior to testing, with gas bubbles forming and departing from the surface even when the surface was below the saturation temperature.

## Discussion

**Surface Characterization.** The roughness of the heater surfaces was measured using a Nanovea PS50 noncontact profilometer scanning over a 1 mm × 1 mm area. Measurements were performed at three or more different locations on each heater. Reactor cladding coupons, prefilmed with boehmite, were also studied to relate the roughness of test surfaces to that expected on actual cladding. The measured average arithmetic ($R_a$) and peak roughness ($R_z$) for the heater surfaces and reactor cladding coupons are summarized in Table 4.

Surface wettability was characterized by measuring equilibrium, static advancing, and static receding contact angles with DI water. Measurements were made using a KSV Instruments CAM 101 system, consisting of a goniometer, camera, and light source. A 500 $\mu$L GasTight series syringe with 22 gauge needle was used to dispense droplets. For equilibrium contact angles, a droplet volume of 2.5–5 $\mu$L was used. Static advancing and static receding angles were determined using the dispensing/withdrawing technique. Contact angles were measured immediately after solvent cleaning and drying using the aforementioned approach.

Contact angles were measured on both plain 6061-T6 aluminum (with the native surface oxide) and the boehmite prefilmed cladding coupons to relate the wettability of these surfaces to the actual heaters used in the study. The 6061-T6 surface with the native oxide exhibited an average sessile drop contact angle of 86°, while the average on the prefilmed cladding surface was 48°.

Contact angles measured on the nominal heater surface prior to boiling are depicted in Figs. 13 and 14, with all results summarized in Table 5. Equilibrium contact angles were also measured following ONB tests and were found to decrease slightly from pretest values to an average of 76° ± 2°.

**Table 4  Summary of measured surface roughness parameters for prefilmed MTR cladding coupons and heater plates used in this study**

| Surface | $R_a$ ($\mu$m) | $R_z$ ($\mu$m) |
|---|---|---|
| Prefilmed MTR cladding coupons | 0.507 ± 0.162 | 3.305 ± 0.985 |
| Heater plates for ONB experiments | 0.486 ± 0.111 | 2.587 ± 0.737 |

**Table 5  Summary of contact angles for the heater surfaces tested**

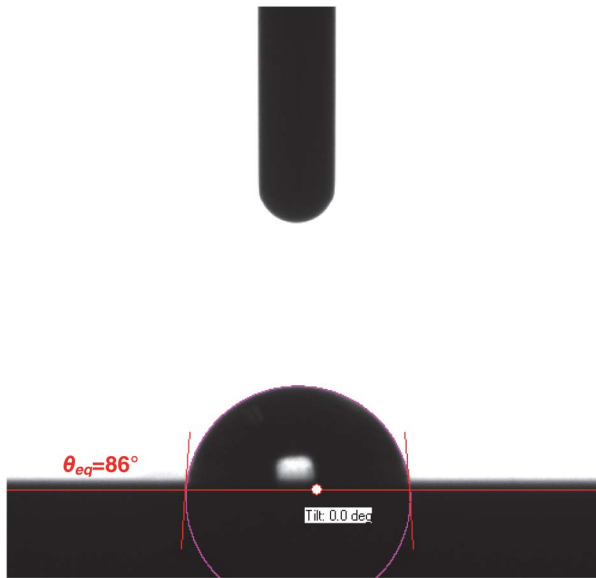|  | Nominal (native oxide) heater surface | Heavily oxidized heater surface |
|---|---|---|
| Equilibrium | 85° ± 3° | 52° ± 5° |
| Static advancing | 95° ± 3° | 58° ± 6° |
| Static receding | 24° ± 3° | 22° ± 2° |



**Fig. 13  Equilibrium contact angle of DI water on the nominal heater surface**

On the heavily oxidized surface, nearly perfect wetting was observed immediately after removal from the furnace (and being allowed to cool to room temperature). This was likely due to burn-off of hydrocarbon contaminants that solvents cannot remove [28]. The surface was allowed to age for several days in air (i.e., accumulate the stable contaminant overlayer), as this was most representative of the actual surface tested. Solvent cleaning was performed immediately before measuring the contact angles, which are shown in Figs. 15 and 16.

From the measurements, it is apparent that the oxidation treatment results in a modest reduction in the contact angle. This contact angle reduction is the suspected cause of the delay in incipience. Therefore, the prefilmed cladding, which has reduced contact angle compared to 6061 aluminum with the native surface oxide, would be expected to have a higher ONB heat flux.
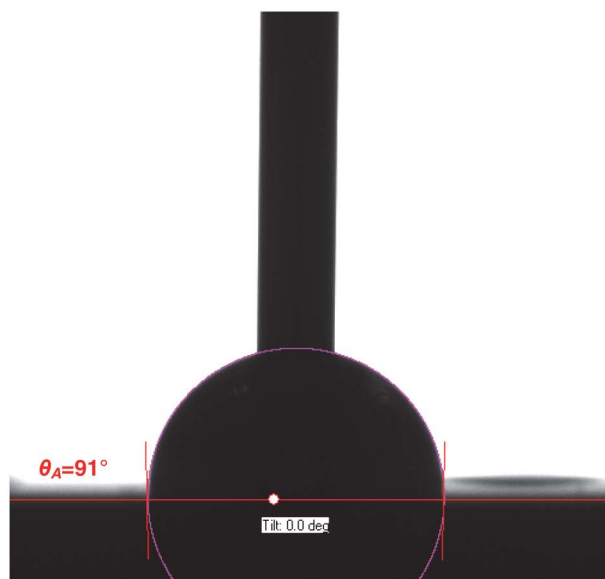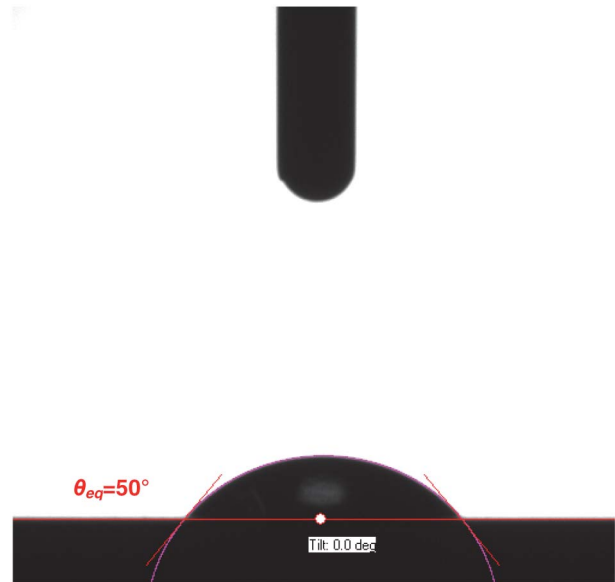


**Fig. 15  Equilibrium contact angle of DI water on the heavily oxidized heater surface**

**Comparison With Existing Correlations.** Results for ONB are plotted in Fig. 17 against several models described previously. The Davis–Anderson correlation (Eq. (17)) is plotted for the measured equilibrium contact angles on the nominal and oxidized



**Fig. 14  Static advancing contact angle (left) and static receding contact angle (right) on the nominal heater surface**

**Fig. 16** Static advancing contact angle (left) and static receding contact angle (right) on the heavily oxidized heater surface

surfaces. While Kandlikar advocates the use of the receding contact angle, in the Davis–Anderson prediction the equilibrium contact angle is most appropriate, as their analysis was conducted for a static bubble on the heated surface.

The error bars represent the measurement uncertainty for the heat flux and associated saturation superheat. Note that a small change in the surface heat flux will lead to a change of the surface temperature of a few degrees or more, which represents a large change in the saturation superheat. Therefore, the experimentally determined saturation superheat at the point of ONB is very sensitive to the exact selection criteria for boiling incipience (i.e., the partition heat flux criteria) and the inherent uncertainty associated with this method. Nonetheless, the experimentally determined saturation superheat for the nominal surface at the point of incipience is in reasonable agreement with the Bergles–Rohsenow model, except at the lowest mass flux condition when $G = 750$ kg/m$^2$ s. At the lowest mass flux ($G = 750$ kg/m$^2$ s), flow likely falls in the transition regime, thereby requiring higher superheats than predicted for initial nucleation due to variation in the boundary layer thickness.
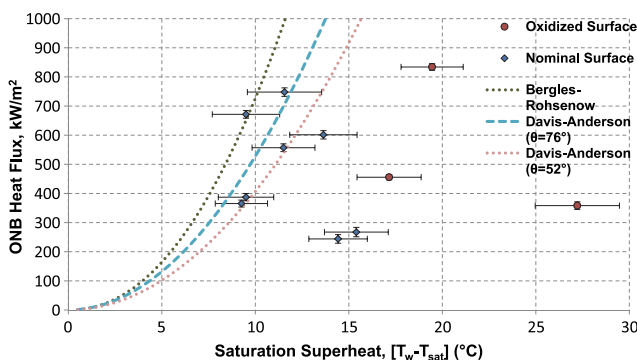


**Fig. 17** ONB heat flux versus wall saturation superheat for all tests conducted with $T_{bulk,in} = 80°C$. In this plot, the Davis–Anderson correlation is shown using the two different equilibrium contact angles measured on the nominal and oxidized surfaces

In typical applications, the surface temperature is unknown, and must be predicted using an appropriate single-phase heat transfer correlation in combination with the chosen model for ONB. In most cases, the result is a transcendental equation that cannot be solved explicitly, but rather the solution can be found through an iterative scheme. As this is the calculation method for the MITR, it may be more appropriate to compare the measured heat flux at ONB to that predicted with the incipience model in combination with the single-phase heat transfer correlation. For the one-sided heating condition, which is representative of a side channel in the MITR and similar MTRs, it has been demonstrated that the Dittus–Boelter (McAdams) correlation is not appropriate. Instead, a new single-phase heat transfer correlation was developed [26]

$$\text{Nu} = \frac{0.199(\text{Re} - 600)^{7/8} \, \text{Pr}}{5[\text{Pr} - 2]\phi^{*1/8} + 10.05(\text{Re} - 600)^{1/8}\phi^{*1/4}} \quad (22)$$

which is applicable for $4000 < \text{Re} < 70{,}000$ and $2.2 < \text{Pr} < 5.4$. $\phi^*$ is a geometry parameter that depends on the channel aspect ratio. Using this equation in conjunction with that of Bergles and Rohsenow (Eq. (10)), the ONB heat flux can be predicted for the experimental conditions and compared to the measured values. This comparison is provided for both the nominal and heavily oxidized surface in Fig. 18. The error bars represent the estimated combined 95% uncertainty associated with the heat flux partition method used to identify incipience. As seen in the figure, the oxidized surface exhibits an 18–40% higher heat flux at ONB compared to the plain surface. The contact angle reduction of about 30° is the probable cause of the increased heat flux needed for incipience.

Using the pressure fluctuation approach to identify the ONB heat flux results in a slightly larger deviation from predicted values, as seen in Fig. 19. Measured values tend to fall lower than predicted, possibly due to the detection of boiling at the edge of the heater. At the very edge of the heater, the influence of the side walls results in a lower fluid velocity, and edge effects from the interface between the heater plate and insulator may play a role in initial nucleation. Whereas the thermocouples, which are located at the axial centerline of the heater, are sufficiently removed not to be influenced by edge effects; the pressure fluctuation method is sensitive to boiling anywhere in the channel. Predicted values are based upon the heater centerline and may not completely account for conditions at the
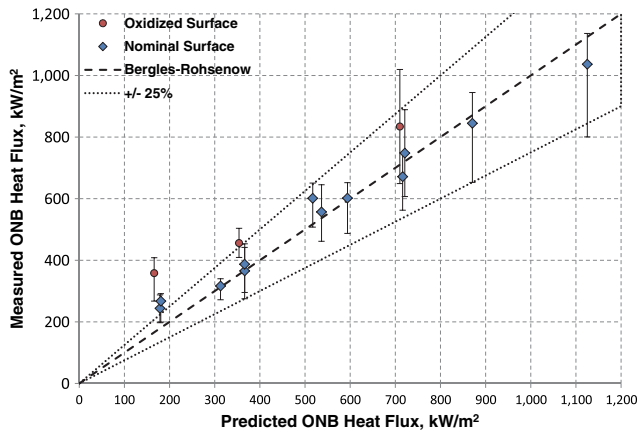
**Fig. 18 Measured ONB heat flux versus that predicted using the Bergles–Rohsenow correlation along with the single-phase heat transfer correlation developed for narrow rectangular channels heated on one side (Eq. (22))**
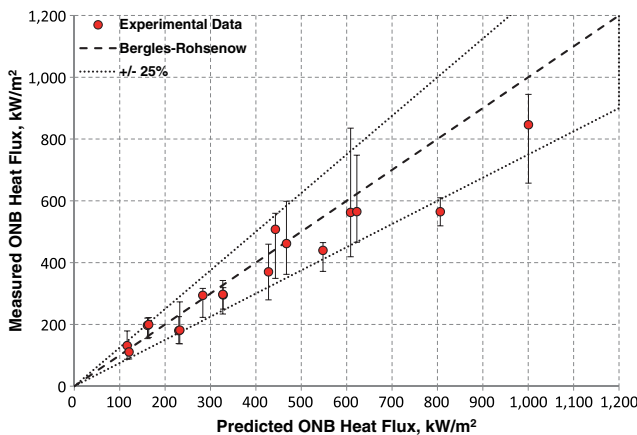


**Fig. 19 Measured ONB heat flux from pressure measurement fluctuations versus that predicted at outlet conditions using the model of Bergles and Rohsenow and Eq. (22)**

heater edge. Therefore, the somewhat lower measured value of the ONB heat flux is expected due to the probable influence of boiling at the heater edges. The pressure fluctuation method might best be characterized as a "global" ONB detection technique.

## Conclusions

This study has explored ONB in a prototypic MTR coolant channel. When relying on analytical correlations to predict the incipience point under forced convection, predictions will depend on the bubble model (hemispherical, truncated sphere, spherical, etc.) along with the required height of the thermal layer (tip of bubble, stagnation point, etc.). Some models, such as that of Davis and Anderson or Kandlikar, account for contact angle due to its effect on the bubble height. Most models assume that a wide range of cavity sizes is available such that the optimum cavity size is present and therefore may not be applicable to very smooth or polished surfaces.

The experimental data indicate that the incipience point during testing is not obvious, and the identification technique used can significantly affect the result. Overall, the temperature measurement

technique using a heat flux partition produced the most reliable and consistent results across all subcoolings and mass fluxes, and is recommended for future comparison. For the surface with the native oxide (nominal surface), results indicate that the Bergles and Rohsenow correlation adequately predicts the ONB heat flux to within ±25% as long as the appropriate single-phase heat transfer correlation is used to predict the surface temperature. However, the oxidized surface, displaying a reduction in the contact angle of about 30°, similar to that for boehmite prefilmed cladding, showed a modest increase in the ONB heat flux. Further reductions in the contact angle are expected to increase the heat flux at which ONB occurs.

The large inherent uncertainty associated with the incipience point, along with the strong dependence on measurement technique and surface condition, undermines the suitability of ONB as a robust safety limit in MTRs. Onset of significant voiding, onset of flow instability, and the critical heat flux can be identified and measured with greater certainty, offering a means of reducing margins while maintaining conservatism.

## Nomenclature

$\mathrm{Co}$ = confinement number, $\equiv \dfrac{\sqrt{\sigma / [g(\rho_l - \rho_v)]}}{D_{\mathrm{hy}}}$

$c_p$ = specific heat capacity, $\mathrm{J/kg\,K}$

$D_{\mathrm{hy}}$ = hydraulic equivalent diameter, m

$G$ = mass flux, $\mathrm{kg/m^2\,s}$

$g$ = gravitational acceleration, $\mathrm{m/s^2}$

$h$ = heat transfer coefficient, $\mathrm{W/m^2\,K}$

$h_{\mathrm{fg}}$ = latent heat of vaporization, $\mathrm{J/kg\,K}$

$k$ = thermal conductivity, $\mathrm{W/m\,K}$

$\mathrm{Nu}$ = Nusselt number, $\equiv \dfrac{h D_{\mathrm{hy}}}{k}$

$P$ = pressure (Pa unless otherwise noted)

$\mathrm{Pr}$ = Prandtl number, $\equiv \dfrac{\mu c_p}{k}$

$q''$ = heat flux, $\mathrm{W/m^2}$

$R$ = specific gas constant, $\mathrm{J/kg\,K}$

$R_a$ = arithmetic average surface roughness, ISO 4287:1997, $\mu m$

$R_z$ = peak roughness, ISO 4287:1997, $\mu m$

$\mathrm{Re}$ = Reynolds number, $\equiv \dfrac{\rho u D_{\mathrm{hy}}}{\mu}$

$r$ = radius, m

$T$ = temperature, K or °C

$t$ = time, s

$u$ = velocity, m/s
$v$ = specific volume, m$^3$/kg
$y$ = height or thickness coordinate, m
$z$ = axial coordinate, m
$z^+$ = dimensionless hydrodynamic position, $\equiv z/D_{hy}$

**Greek Letters**
$\beta$ = dynamic receding contact angle, degrees
$\Delta$ = difference
$\delta$ = layer thickness, m
$\theta$ = contact angle, degrees
$\mu$ = viscosity, Pa s
$\rho$ = density, kg/m$^3$
$\sigma$ = surface tension, N/m
$\phi^*$ = geometry function

**Subscripts/Superscripts**
A = advanced
b = bubble
bulk = bulk fluid
c = cavity
crit = critical
eq = equilibrium
l = liquid
ONB = onset of nucleate boiling
R = receded
sat = saturation
shl = superheated layer
stag = stagnation point
sub = subcooling
th = thermal
v = vapor
ve = vapor embryo
w = wall

**Acronyms**
ATR = advanced test reactor
DI = deionized
GTRI = Global Threat Reduction Initiative
HEU = high-enriched uranium
HPRR = high-performance research reactor
LEU = low-enriched uranium
LSSS = limiting safety system setting
MITR = MIT research reactor
MTR = materials test reactor
ONB = onset of nucleate boiling
RSD = relative standard deviation

## References

[1] MITR Staff, 2011, "Safety Analysis Report for the MIT Research Reactor," Massachusetts Institute of Technology, Cambridge, MA, Report No. MIT-NRL-11-02.

[2] Bergles, A. E., and Rohsenow, W. M., 1964, "The Determination of Forced-Convection Surface-Boiling Heat Transfer," J. Heat Transfer, **86**(3), pp. 365–372.

[3] McAdams, W. H., 1942, *Heat Transmission*, 2nd ed., McGraw-Hill, New York, NY, pp. 167–168.

[4] Bankoff, S. G., 1958, "Entrapment of a Gas in the Spreading of a Liquid Over a Rough Surface," AI ChE J., **4**(1), pp. 24–26.

[5] Jones, S. F., Evans, G. M., and Galvin, K. P., 1999, "Bubble Nucleation From Gas Cavities—A Review," Adv. Colloid Interface Sci., **80**(1), pp. 27–50.

[6] Eddington, R. I., and Kenning, D. B. R., 1979, "The Effect of Contact Angle on Bubble Nucleation," Int. J. Heat Mass Transfer, **22**(8), pp. 1231–1236.

[7] Tong, W., Bar-Cohen, A., Simon, T. W., and You, S. M., 1990, "Contact Angle Effects on Boiling Incipience in Highly-Wetting Liquids," Int. J. Heat Mass Transfer, **33**(1), pp. 91–103.

[8] Pioro, I. L., Rohsenow, W., and Doerffer, S. S., 2004, "Nucleate Pool-Boiling Heat Transfer. I: Review of Parametric Effects on Boiling Surface," Int. J. Heat Mass Transfer, **47**(23), pp. 5033–5044.

[9] Carey, V. P., 2008, *Liquid-Vapor Phase-Change Phenomena*, 2nd ed., Taylor & Francis Group, LLC, New York, NY, pp. 164–172.

[10] Hsu, Y. Y., and Graham, W., 1961, "An Analytical and Experimental Study of the Thermal Boundary Layer and Ebullition Cycle in Nucleate Boiling," NASA, Technical Note No. D-594.

[11] Hsu, Y. Y., 1962, "On the Size Range of Active Nucleation Cavities on a Heating Surface," J. Heat Transfer, **84**(3), pp. 207–216.

[12] Satō, T., and Matsumura, H., 1964, "On the Conditions of Incipient Subcooled-Boiling With Forced Convection," Bull. J. Soc. Mech. Eng., **7**(26), pp. 329–338.

[13] Davis, E. J., and Anderson, G. H., 1966, "The Incipience of Nucleate Boiling in Forced Convection Flow," AIChE J., **12**(4), pp. 774–780.

[14] Kandlikar, S. G., 2006, *Heat Transfer and Fluid Flow in Minichannels and Microchannels*, Elsevier, Amsterdam, pp. 175–181.

[15] Kandlikar, S. G., Mizo, V., Cartwright, M., and Ikenze, E., 1997, "Bubble Nucleation and Growth Characteristics in Subcooled Flow Boiling of Water," ASME Proceedings of the 32nd National Heat Transfer Conference, American Society of Mechanical Engineers, New York, Vol. **4**, pp. 11–18.

[16] Sudo, Y., Miyata, K., Ikawa, H., and Kaminaga, M., 1986, "Experimental Study of Incipient Nucleate Boiling in Narrow Vertical Rectangular Channel Simulating Subchannel of Upgraded JRR-3," J. Nucl. Sci. Technol., **23**(1), pp. 73–82.

[17] Hong, G., Yan, X., Yang, Y. H., Liu, S., and Huang, Y. P., 2012, "Experimental Study of Onset of Nucleate Boiling in a Narrow Rectangular Channel Under Static and Heaving Conditions," Ann. Nucl. Energy, **39**(1), pp. 26–34.

[18] Wang, J., Huang, Y., and Wang, Y., 2011, "Visualized Study on Specific Points on Demand Curves and Flow Patterns in a Single-Side Heated Narrow Rectangular Channel," Int. J. Heat Fluid Flow, **32**(5), pp. 982–992.

[19] Wu, Y. W., Su, G. H., Hu, B. X., and Qiu, S. Z., 2010, "Study of Onset of Nucleate Boiling in Bilaterally Heated Narrow Annuli," Int. J. Therm. Sci., **49**(5), pp. 741–748.

[20] Bergles, A. E., and Rohsenow, W. M., 1962, "Forced Convection Surface-Boiling Heat Transfer and Burnout in Tubes of Small Diameter," Massachusetts Institute of Technology, Report No. 8767-21Air Force Contract AF 19(604)-7344.

[21] Kennedy, J. E., Roach, G. M., Jr., Dowling, M. F., Abdel-Khalik, S. I., Ghiaasiaan, S. M., Jeter, S. M., and Quershi, Z. H., 2000, "The Onset of Flow Instability in Uniformly Heated Horizontal Microchannels," J. Heat Transfer, **122**(1), pp. 118–125.

[22] Collier, J. G., and Thome, J. R., 1994, *Convective Boiling and Condensation*, 3rd ed., Clarendon Press, Oxford, pp. 186–196.

[23] McAdams, W. H., Kennel, W. E., Minden, C. S., Carl, R., Picornell, P. M., and Dew, J. E., 1949, "Heat Transfer at High Rates to Water with Surface Boiling," Ind. Eng. Chem., **41**(9), pp. 1945–1953.

[24] You, S. M., Simon, T. W., and Bar-Cohen, A., 1995, "Effects of Dissolved Gas Content on Pool Boiling of a Highly Wetting Fluid," J. Heat Transfer, **117**(3), pp. 687–692.

[25] Rainey, K. N., You, S. M., and Lee, S., 2003, "Effect of Pressure, Subcooling, and Dissolved Gas on Pool Boiling Heat Transfer From Microporous Surfaces in FC-72," J. Heat Transfer, **125**(1), pp. 75–83.

[26] Forrest, E. C., Hu, L. W., Buongiorno, J., and McKrell, T. J., "Convective Heat Transfer in a High Aspect Ratio Mini-Channel Heated on One Side," J. Heat Transfer. (submitted)

[27] Kline, S. J., and McClintock, F. A., 1953, "Describing Uncertainties in Single-Sample Experiments," Mech. Eng., **75**(Jan), pp. 3–8.

[28] Forrest, E., Schulze, R., Liu, C., and Dombrowski, D., 2015, "Influence of Surface Contamination on the Wettability of Heat Transfer Surfaces," Int. J. Heat Mass Transfer, **91**, pp. 311–317.